Prediction of Vibration Behavior of Micro-Circular Disks at Low Reynolds Number Regime

Adil El Baroudi*

Arts et Métiers ParisTech, 2 boulevard du Ronceray
49035 Angers, France
adil.elbaroudi@ensam.eu

Fulgence Razafimahery

IRMAR
Université de Rennes 1, Campus de Beaulieu
35042 Rennes Cedex, France

In the current study, a theoretical method is developed to predict the vibrational behavior of micro-circular disks filled with viscous fluids and numerical results are presented to validate the model. Vibrations with two outer boundary conditions, rigid and deformable vessel, are studied. The coupled governing equations of both rigid and deformable vessel vibration are solved by the analytical procedure, taking fluid–structure interaction into account. The fluid gap effect on the coupled eigenfrequencies is also considered. The frequency spectrum plots of the first several eigenfrequencies are presented in a wide range of fluid gap and elasticity ratio. The correctness of results is demonstrated using a commercial finite element software. It is shown that the obtained results through the proposed method reveal very good agreement with the numerical solution.

Keywords: Elasto-viscous interaction; two-dimensional coupled vibration; micro-circular structures; finite element method.

1. Introduction

Structures filled with fluids and fluids surrounding structures have been gaining momentum in engineering. Paidoussis[1,2] revealed that this configuration is fast able to exhibit richer dynamic and modal behaviors than the standard model of the structure exposed to compressive loads. Due to the recent developments in science and technology, the structures dimensions could get smaller. Therefore, microscale structures have held wide range of applications in engineering microfluidic devices and microelectronic-mechanical systems. In addition, implementing the microfluidic–microstructure

*Corresponding author.

interaction analysis into the engineering and biological systems could be because of its inherent attributes related to the modeling of the rigid and flexible microstructures which are geometrically complex in nature. To study such phenomena, the task is to choose suitable fluid models and structural models depending on the application and to develop an efficient interface to couple them.

On the one hand, microstructures and microfluidics promise a great deal of advantages in the field of drug discovery like low sample consumption and analysis or experiment times.[3] Like any other technology, to be able to implement micro-structures and microfluidic,[4,5] suitable production techniques have to be discovered. Microstructures and microfluidics systems can have various applications in micro-resonators[6] and in targeted drug delivery devices and, in view of their excellent mechanical properties and hollow geometry. Bhirde[7] showed that the hollow geometry, for example, can be considered as drug delivery system in targeted therapy which results in a significant decrease in tumor size.

On the other hand, vascular cell biology is a field in which extensive research is being carried out due to its relevance in biomedicine. The main obstacle is that it is difficult to mimic the functioning of valve tissue.[8] Biology cells are encapsulated by a membrane composed of a lipid bilayer attached to a polymer network underlying. In order to understand and distinguish the features of cell mechanics that arise from the components of the cell membrane, particles enclosed by a lipid bilayer (vesicles)[9,10] or a polymerized membrane (artificial capsules)[11] have been studied extensively by theory and simulations.[12–14] Microstructures and microfluidics show great potential to enable a systematic study of vascular cell biology.

Much of the early research in this domain has been focused on the internal fluid's behavior flows through micro-tubes. Understanding of the inner fluid flow is currently a topic of great interest in development of engineering devices and biological systems at the small scales. Accordingly, a rigorous understanding of the in-plane vibration behavior of micro-circular disks filled with viscous fluids is particularly relevant. In spite of many contributions regarding the analysis of micro-circular disks, the establishment of an efficient and reliable mathematical model to be able to predict vibrational behavior of micro-circular disks taking into account fluid–structure interaction remains a daunting task and is the purpose of the present paper. This article attempts to develop a theoretical method whose main objective is to calculate the natural frequencies of a micro-circular disks submerged in a fluid-filled rigid and deformable tube (vessel). In the theoretical formulation, the fluid in the annular space between the micro-disk (micro-structure) and vessel, and the fluid inside the micro-disk would both be considered.

2. Mathematical Modeling

2.1. *Formulation for compressible viscous fluids*

Consider a viscous compressible fluid between two concentric elastic micro-disks (elastic vessel and elastic structure) of radii $r = a_2$ and $r = a_4$ (see Fig. 1). When the

micro-structure is completely immersed in a fluid-filled elastic vessel, the fluid domain is divided into two sub-domains, inner region and outer region. The two configurations are inspected. One is only the outer fluid-filled case, and the other is the case that the micro-structure is in contact simultaneously with inner fluid and outer fluid. It is convenient to use polar coordinates (r, θ) with origins at the center of the micro-disks. Each micro-disk (micro-structure and micro vessel) may execute harmonic motion with angular frequency ω. The oscillation amplitude is considered to be small enough to neglect the convective fluid inertial forces. Under these assumptions, the unsteady linear Stokes equation can be used to model the fluid dynamics. Based on the assumption that the fluid is Newtonian, the total stress tensor that combines the viscous stress with pressure is given by

$$\boldsymbol{\sigma}^{(f,i)}(\mathbf{v}^{(i)}, p^{(i)}) = -p^{(i)}\mathbf{I} + 2\eta_i \boldsymbol{\varepsilon}^{(f,i)}(\mathbf{v}^{(i)}) - \frac{2\eta_i}{3}(\nabla \cdot \mathbf{v}^{(i)})\mathbf{I} \qquad (1)$$

and

$$\boldsymbol{\varepsilon}^{(f,i)}(\mathbf{v}^{(i)}) = \frac{1}{2}[\nabla \mathbf{v}^{(i)} + (\nabla \mathbf{v}^{(i)})^T] \qquad (2)$$

is the strain-rate tensor. Here, η_i is the dynamic viscosity, $p^{(i)}$ is the pressure, $\mathbf{v}^{(i)}$ is the velocity vector, $\mathbf{I}$ is an unit tensor and the superscript T denotes the transpose. In addition, $i = 1$ indicates the inner fluid and $i = 2$ the outer fluid. For the acoustic problem when the fluid velocity is small compared to the dimensions of the model, the nonlinear convection term in the Navier–Stokes equation can be neglected. Therefore, from mass and momentum conservation in the absence of body forces, the linearized Navier–Stokes equations of a compressible viscous fluid are governed by[15]

$$\frac{\partial \rho_f^{(i)}}{\partial t} + \rho_f^{(i)} \nabla \cdot \mathbf{v}^{(i)} = 0, \qquad (3)$$

$$\rho_f^{(i)} \frac{\partial \mathbf{v}^{(i)}}{\partial t} - \nabla \cdot \boldsymbol{\sigma}^{(f,i)}(\mathbf{v}^{(i)}, p^{(i)}) = \mathbf{0}, \qquad (4)$$

$$\frac{\partial \rho_f^{(i)}}{\partial p^{(i)}} = \frac{1}{c_i^2}, \qquad (5)$$

where $\rho_f^{(i)}$ represents the fluid density and c_i is the speed of sound in a fluid domain. Equation (5) is the definition of the compressibility. Note that for acoustic problem, a small variations in fluid density $\rho_f^{(i)}$ causes a small variations in fluid pressure $p^{(i)}$ by rapid adiabatic process. In order to plainly show how the new set of partial differential equations is derived, as in Ref. 16, we decompose using a traditional Helmholtz decomposition into compressible and solenoidal parts as $\mathbf{v}^{(i)} = \nabla \phi^{(i)} + \nabla \times \boldsymbol{\Psi}^{(i)}$. Note that the potential component $\nabla \phi^{(i)}$ (curl-free component) represents dilatational waves and describes the compressible part of the velocity field. The solenoidal component $\nabla \times \boldsymbol{\Psi}^{(i)}$ (divergence-free component) represents shear waves and

describes the incompressible part of the velocity field. The symmetry of problem allows to reduces the vector potential $\boldsymbol{\Psi}^{(i)}$ into scalar potential as $\boldsymbol{\Psi}^{(i)} = (0, 0, \psi^{(i)})$. Furthermore, substituting the above decomposition into Eq. (4), and by making use of Eqs. (3) and (5), the conservation of momentum equation (4) becomes[17]

$$\left(c_i^2 + \frac{4\eta_i}{3\rho_f^{(i)}} \frac{\partial}{\partial t} \right) \nabla^2 \phi^{(i)} = \frac{\partial^2 \phi^{(i)}}{\partial t^2}, \tag{6}$$

$$\eta_i \nabla^2 \psi^{(i)} = \rho_f^{(i)} \frac{\partial \psi^{(i)}}{\partial t}, \tag{7}$$

$$p^{(i)} = \frac{4\eta_i}{3} \nabla^2 \phi^{(i)} - \rho_f^{(i)} \frac{\partial \phi^{(i)}}{\partial t}. \tag{8}$$

In the present study, both analytical and numerical methods are used to solve the problem under consideration. The resolution procedure starts with finding the analytical solution, then the eigenvalue equation is obtained from the appropriate boundary and interface conditions. Finally, the numerical solution is computed using Comsol Multiphysics software. In order to solve the free vibration problem, a time harmonic dependence $\exp(j\omega t)$ is assumed, with j is the imaginary unit and t the time. The two subproblems consist of determining the scalar potentials $\phi^{(i)}(r, \theta, t)$ and $\psi^{(i)}(r, \theta, t)$ satisfying the Helmholtz Eqs. (6) and (7). Introducing a new auxiliary variable $\alpha = j\sqrt{j\omega}$ and using previously developed techniques,[18] the general solution associated with circumferential modal number n can be expressed as

$$\begin{Bmatrix} \phi^{(i)} \\ \psi^{(i)} \\ p^{(i)} \end{Bmatrix} (r, \theta, t) = \begin{Bmatrix} \phi^{(i)}(r)[a\sin(n\theta) + b\cos(n\theta)] \\ {}^{(i)}(r)[c\cos(n\theta) + d\sin(n\theta)] \\ p^{(i)}(r)[a\sin(n\theta) + b\cos(n\theta)] \end{Bmatrix} \exp(j\omega t), \tag{9}$$

where the radial dependence is defined as

$$\phi^{(i)}(r) = A_f^{(i)} J_n(\beta_i r) + B_f^{(i)} Y_n(\beta_i r),$$

$${}^{(i)}(r) = C_f^{(i)} J_n\left(\frac{\alpha r}{\sqrt{\nu_i}} \right) + D_f^{(i)} Y_n\left(\frac{\alpha r}{\sqrt{\nu_i}} \right),$$

and the radial dependence of pressure is obtained from Eq. (8) as

$$p^{(i)}(r) = \eta_i \left(\frac{\alpha^2}{\nu_i} - \frac{4\beta_i^2}{3} \right) [A_f^{(i)} J_n(\beta_i r) + B_f^{(i)} Y_n(\beta_i r)].$$

In the above equations, $\alpha/\sqrt{\nu_i}$ is the shear wavenumber where ν_i is the kinematic viscosity, $\beta_i^2 = \alpha^4/(4\nu_i\alpha^2/3 - c_i^2)$, J_n and Y_n are, respectively, the nth order standard Bessel function of the first and the second kind; whereas $A_f^{(i)}, B_f^{(i)}, C_f^{(i)}$ and $D_f^{(i)}$ are unknown wave propagation coefficients. Note that the components of velocity field are symmetric or antisymmetric in θ. Because of the periodicity, the azimuthal

modes corresponding to $\cos(n\theta)$ and $\sin(n\theta)$ are really the same, i.e., for the two families there is no difference in the values of n. We proceed (for convenience) with the terms involving $\sin(n\theta)$ for $\phi^{(i)}$, $\cos(n\theta)$ for $\psi^{(i)}$ and scale the constants with a and c. The components of velocity in the fluid region that are used lastly in boundary condition are given by

$$\left\{ \begin{array}{c} v_r^{(i)} \\ v_\theta^{(i)} \end{array} \right\} (r,\theta,t) = \left\{ \begin{array}{c} \left[\phi^{(i)\prime}(r) - \dfrac{n}{r}\psi^{(i)}(r) \right] \sin(n\theta) \\ \left[\dfrac{n}{r}\phi^{(i)}(r) - \psi^{(i)\prime}(r) \right] \cos(n\theta) \end{array} \right\} \exp(j\omega t), \qquad (10)$$

where the prime signifies differentiation with respect to the argument r. Then, the pertinent stress-potentials expressions can be obtained by direct substitution of the expansions (10) into the constitutive equation (1) as follows:

$$\left\{ \begin{array}{c} \sigma_{rr}^{(f,i)} \\ \sigma_{r\theta}^{(f,i)} \end{array} \right\} (r,\theta,t) = \left\{ \begin{array}{c} \sigma_{rr}^{(f,i)}(r)\sin(n\theta) \\ \sigma_{r\theta}^{(f,i)}(r)\cos(n\theta) \end{array} \right\} \exp(j\omega t), \qquad (11)$$

where the radial dependence $\sigma_{rr}^{(f,i)}(r)$ and $\sigma_{r\theta}^{(f,i)}(r)$ are defined as

$$\sigma_{rr}^{(f,i)} = 2\eta_i \left\{ \phi^{(i)\prime\prime}(r) + \left(\beta_i^2 - \frac{\alpha^2}{2\nu_i} \right)\phi^{(i)}(r) - \frac{n}{r^2}\left[r\psi^{(i)\prime}(r) - \psi^{(i)}(r) \right] \right\},$$

$$\sigma_{r\theta}^{(f,i)} = 2\eta_i \left\{ \frac{n}{r^2}\left[r\phi^{(i)\prime}(r) - \phi^{(i)}(r) \right] - \psi^{(i)\prime\prime}(r) - \frac{\alpha^2}{2\nu_i}\psi^{(i)}(r) \right\}.$$

2.2. *Formulation for elastic micro-discs*

The micro-disks under consideration are assumed to be linearly elastic (isotropic) for which the constitutive equation may be written as

$$\boldsymbol{\sigma}^{(s,i)}(\mathbf{u}^{(i)}) = \lambda_i(\nabla \cdot \mathbf{u}^{(i)})\mathbf{I} + \mu_i[\nabla\mathbf{u}^{(i)} + \nabla\mathbf{u}^{(i)T}], \qquad (12)$$

where $\mathbf{u}^{(i)}$ is the displacement field, (λ_i, μ_i) are Lamé constants and $i = 1$ indicates the elastic micro-structure and $(i = 2)$ the elastic micro-vessel. The problem can be analyzed by means of the standard methods of elastodynamics. For deriving the partial differential equations, the Navier's equation in the absence of body forces can be expressed as

$$\rho_s^{(i)}\frac{\partial^2 \mathbf{u}^{(i)}}{\partial t^2} = \nabla \cdot \boldsymbol{\sigma}^{(s,i)}(\mathbf{u}^{(i)}), \qquad (13)$$

where $\mathbf{u}^{(i)}$ can advantageously be decomposed using again Helmholtz decomposition with two scalar potential functions $\Phi^{(i)}$ and $\Psi^{(i)}$. This decomposition enables us to separate the Navier's equation (13) in terms of two classical wave equations

$$(\nabla^2 - k_L^{(i)2})\Phi^{(i)} = 0, \quad (\nabla^2 - k_T^{(i)2})\Psi^{(i)} = 0, \qquad (14)$$

where $k_L^{(i)} = \alpha^2\sqrt{\rho_s^{(i)}/(\lambda_i + 2\mu_i)}$ and $k_T^{(i)} = \alpha^2\sqrt{\rho_s^{(i)}/\mu_i}$ are the radial and shear wave numbers and $\rho_s^{(i)}$ is the micro-discs materials density. Hence, using previously developed techniques,[18] the general solution of Eqs. (14) can be shown to be

$$\left\{\begin{array}{c} \Phi^{(i)} \\ \Psi^{(i)} \end{array}\right\}(r,\theta,t) = \left\{\begin{array}{c} \Phi^{(i)}(r)\sin(n\theta) \\ \Psi^{(i)}(r)\cos(n\theta) \end{array}\right\}\exp(j\omega t), \tag{15}$$

where $\Phi^{(i)}(r)$ and $\Psi^{(i)}(r)$ are defined as

$$\Phi^{(i)}(r) = A_s^{(i)}I_n(k_L^{(i)}r) + B_s^{(i)}K_n(k_L^{(i)}r),$$
$$\Psi^{(i)}(r) = C_s^{(i)}I_n(k_T^{(i)}r) + D_s^{(i)}K_n(k_T^{(i)}r).$$

Here, I_n and K_n are modified Bessel function of the first and second kind; $A_s^{(i)}, B_s^{(i)}$, $C_s^{(i)}, D_s^{(i)}$ are unknown coefficients to be determined by the boundary and interface conditions. In the end, the components of displacement that used lastly in boundary condition can be expressed as

$$\left\{\begin{array}{c} u_r^{(i)} \\ u_\theta^{(i)} \end{array}\right\}(r,\theta,t) = \left\{\begin{array}{c} \left[\Phi^{(i)\prime}(r) - \dfrac{n}{r}\Psi^{(i)}(r)\right]\sin(n\theta) \\ \left[\dfrac{n}{r}\Phi^{(i)}(r) - \Psi^{(i)\prime}(r)\right]\cos(n\theta) \end{array}\right\}\exp(j\omega t). \tag{16}$$

Consequently, the pertinent stress-potentials expressions can be obtained by direct substitution of the expansions (16) into the constitutive equation (12) as follows:

$$\left\{\begin{array}{c} \sigma_{rr}^{(s,i)} \\ \sigma_{r\theta}^{(s,i)} \end{array}\right\}(r,\theta,t) = \left\{\begin{array}{c} \sigma_{rr}^{(s,i)}(r)\sin(n\theta) \\ \sigma_{r\theta}^{(s,i)}(r)\cos(n\theta) \end{array}\right\}\exp(j\omega t), \tag{17}$$

where $\sigma_{rr}^{(s,i)}(r)$ and $\sigma_{r\theta}^{(s,i)}(r)$ are defined as

$$\sigma_{rr}^{(s,i)}(r) = \mu_i\left\{2\Phi^{(i)\prime\prime}(r) + \frac{\lambda_i k_L^{(i)2}}{\mu_i}\Phi^{(i)}(r) - \frac{2n}{r^2}[r\Psi^{(i)\prime}(r) - \Psi^{(i)}(r)]\right\},$$

$$\sigma_{r\theta}^{(s,i)}(r) = \mu_i\left\{\frac{2n}{r^2}[r\Phi^{(i)\prime}(r) - \Phi^{(i)}(r)] - 2\Psi^{(i)\prime\prime}(r) + k_T^{(i)2}\Psi^{(i)}(r)\right\}.$$

2.3. *Boundary conditions and eigenvalue equation*

At this point, the free vibration frequencies of the coupled system shall be obtained by application of the pertinent boundary and interface conditions. Therefore, the fluid–structure coupling takes place at the interfaces $r = a_1$ (Γ_1), $r = a_2$ (Γ_2) and $r = a_3$ (Γ_3). Kinematic and dynamic continuity have to be ensured across these interfaces. Thus, the fluid–structure coupling concerning the fluid is of

nonhomogeneous Dirichlet condition (kinematic condition)

$$\text{at } r = a_1, \quad v_r^{(1)} = \frac{\partial u_r^{(1)}}{\partial t}, \quad v_\theta^{(1)} = \frac{\partial u_\theta^{(1)}}{\partial t},$$

$$\text{at } r = a_2, \quad v_r^{(2)} = \frac{\partial u_r^{(1)}}{\partial t}, \quad v_\theta^{(2)} = \frac{\partial u_\theta^{(1)}}{\partial t}, \tag{18}$$

$$\text{at } r = a_3, \quad v_r^{(2)} = \frac{\partial u_r^{(2)}}{\partial t}, \quad v_\theta^{(2)} = \frac{\partial u_\theta^{(2)}}{\partial t},$$

describing mass conservation across the interface, and the fluid–structure coupling for the micro-discs is of nonhomogeneous Neumann type (dynamic condition)

$$\text{at } r = a_1, \quad \sigma_{rr}^{(f,1)} = \sigma_{rr}^{(s,1)}, \quad \sigma_{r\theta}^{(f,1)} = \sigma_{r\theta}^{(s,1)},$$

$$\text{at } r = a_2, \quad \sigma_{rr}^{(f,2)} = \sigma_{rr}^{(s,1)}, \quad \sigma_{r\theta}^{(f,2)} = \sigma_{r\theta}^{(s,1)}, \tag{19}$$

$$\text{at } r = a_3, \quad \sigma_{rr}^{(f,2)} = \sigma_{rr}^{(s,2)}, \quad \sigma_{r\theta}^{(f,2)} = \sigma_{r\theta}^{(s,2)},$$

representing the equivalence of micro-disks stresses $\sigma^{(s,i)}$ and fluid stresses $\sigma^{(f,i)}$. These conditions are not sufficient in order to have a fully described system. To complete the boundary conditions, the stress free condition for the outside surface (Γ_4) considered in this work is specified as follows:

$$\text{at } r = a_4, \quad \sigma_{rr}^{(s,2)} = 0, \quad \sigma_{r\theta}^{(s,2)} = 0. \tag{20}$$

Note that in the case of deformable vessel, fourteen boundary conditions are needed. Therefore, for a rigid vessel, it is easy to verify that the number of boundary conditions is 10. Thus the solution of Eqs. (3), (4) and (13) is incorporated into the boundary conditions given in Eqs. (18)–(20), which yields an homogeneous system of 14 algebraic equations, where the unknowns are the constants in the expressions for the fluid velocities and the amplitudes of the structure motion

$$\mathbf{M}\mathbf{x} = \mathbf{0}, \tag{21}$$

in which $\mathbf{M}$ can be expressed as

$$\mathbf{M} = \begin{bmatrix} \mathbf{M}_f^{(1)}(a_1) & \mathbf{M}_s^{(1)}(a_1) & \mathbf{0} & \mathbf{0} \\ \mathbf{0} & \mathbf{M}_s^{(1)}(a_2) & \mathbf{M}_f^{(2)}(a_2) & \mathbf{0} \\ \mathbf{0} & \mathbf{0} & \mathbf{M}_f^{(2)}(a_3) & \mathbf{M}_s^{(2)}(a_3) \\ \mathbf{0} & \mathbf{0} & \mathbf{0} & \mathbf{M}_s^{(2)}(a_4) \end{bmatrix}. \tag{22}$$

The elements of the sub-matrices $\mathbf{M}_q^{(i)}(r)$ ($q = f, s$ and $i = 1, 2$) are given in Appendix A. $\mathbf{x}$ is the vector of unknown coefficients and is written as

$$\mathbf{x} = [A_f^{(1)} \ C_f^{(1)} \ A_s^{(1)} \ B_s^{(1)} \ C_s^{(1)} \ D_s^{(1)} \ A_f^{(2)} \ B_f^{(2)} \ C_f^{(2)} \ D_f^{(2)} \ A_s^{(2)} \ B_s^{(2)} \ C_s^{(2)} \ D_s^{(2)}]^T.$$

For the nontrivial solution of Eq. (21), it is required that $\det(\mathbf{M}) = 0$ which is the frequency equation of the coupling system. This frequency equation can be used to investigate the coupled natural frequencies of the system. For given dimensions, elastic and fluid constants of the system, $\det(\mathbf{M}) = 0$ constitutes an implicit transcendental function of n and α. The roots α may be computed for a fixed n.

2.4. *Weak formulation and numerical solution*

The finite element formulation of fluid–structure coupled model presented in this section is based on the formulations for the solids and for compressible viscous fluids. The used numerical formulations include the pressure formulation,[19] the potential formulation,[20] the displacement formulation[21] and the combination of some of them.[22] Finite element procedure is used to extract the natural frequencies. To compute the natural vibration of a fluid alone, the fluid is typically described either by pressure or by displacement potential variables. When the fluid is coupled with a solid, standard methods to solve Eqs. (3), (4) and (13) consist in eliminating either the pressure or the displacement potential.[23] However, in both cases, nonsymmetric eigenvalue problems are obtained (see, for instance, Ref. 24). To avoid this drawback, Morand and Ohayon[25] introduce in Ref. 20 an alternative procedure which consists in using pressure and displacement potential simultaneously. In this section we summarize their approach; further details and discussions can be found in their book.[25]

2.4.1. *Fluid domains*

In order to obtain a weak formulation for Eqs. (3) and (4), firstly replacing fluid density $\rho_f^{(i)}$ by the fluid pressure $p^{(i)}$ using the constitutive Eq. (5) and introducing the fluid displacement $\partial \mathbf{w}^{(i)}/\partial t = \mathbf{v}^{(i)}$, we get $p^{(i)} = -\rho_f^{(i)} c_i^2 \nabla \cdot \mathbf{w}^{(i)}$. Therefore, the Stokes equation and Cauchy stress tensor are written only in terms of the fluid displacements as

$$\rho_f^{(i)} \frac{\partial^2 \mathbf{w}^{(i)}}{\partial t^2} - \nabla \cdot \boldsymbol{\sigma}^{(f,i)}(\mathbf{w}^{(i)}) = 0 \tag{23}$$

and

$$\boldsymbol{\sigma}^{(f,i)}(\mathbf{w}^{(i)}) = \rho_f^{(i)} c_i^2 (\nabla \cdot \mathbf{w}^{(i)})\mathbf{I} + 2\eta_i \frac{\partial}{\partial t} \boldsymbol{\varepsilon}^{(f,i)}(\mathbf{w}^{(i)}) - \frac{2\eta_i}{3} \frac{\partial}{\partial t}(\nabla \cdot \mathbf{w}^{(i)})\mathbf{I}. \tag{24}$$

Note that this pure displacement-based formulation tends to lock for a nearly incompressible fluid.[22]

To derive the weak form of the Stokes equation, following the standard approach and using tensor notation, we multiply Eq. (23) by appropriate momentum test function $\bar{\mathbf{w}}_i$ and integrate over the fluid volume $\Omega_f^{(i)}$ to obtain

$$\int_{\Omega_f^{(i)}} \left[\rho_f^{(i)} \frac{\partial^2 \mathbf{w}^{(i)}}{\partial t^2} - \nabla \cdot \boldsymbol{\sigma}^{(f,i)}(\mathbf{w}^{(i)}) \right] \bar{\mathbf{w}}_i d\Omega = 0. \tag{25}$$

During the interaction, the fluid particle and the structure move together in the normal direction of the boundary. Note that the normal on the interface on the solids $\mathbf{n}_s^{(i)}$ is opposite the normal on the fluid $\mathbf{n}_f^{(i)}$, that is $\mathbf{n}_s^{(i)} = -\mathbf{n}_f^{(i)}$. Integrating by parts the Cauchy-stress term present in the Eq. (25) and taking into account boundary conditions, we get for inner fluid (domain $\Omega_f^{(1)}$)

$$\int_{\Omega_f^{(1)}} \rho_f^{(1)} \frac{\partial^2 \mathbf{w}^{(1)}}{\partial t^2} \bar{\mathbf{w}}_1 d\Omega + \int_{\Omega_f^{(1)}} \boldsymbol{\sigma}^{(f,1)}(\mathbf{w}^{(1)}) : \boldsymbol{\varepsilon}^{(f,1)}(\bar{\mathbf{w}}_1) d\Omega$$

$$+ \int_{\Gamma_1} \boldsymbol{\sigma}^{(f,1)}(\mathbf{w}^{(1)}) \cdot \mathbf{n}_s^{(1)} \bar{\mathbf{w}}_1 d\Gamma = 0, \tag{26}$$

and for outer fluid (domain $\Omega_f^{(2)}$)

$$\int_{\Omega_f^{(2)}} \rho_f^{(2)} \frac{\partial^2 \mathbf{w}^{(2)}}{\partial t^2} \bar{\mathbf{w}}_2 d\Omega + \int_{\Omega_f^{(2)}} \boldsymbol{\sigma}^{(f,2)}(\mathbf{w}^{(2)}) : \boldsymbol{\varepsilon}^{(f,2)}(\bar{\mathbf{w}}_2) d\Omega$$

$$+ \int_{\Gamma_2} \boldsymbol{\sigma}^{(f,2)}(\mathbf{w}^{(2)}) \cdot \mathbf{n}_s^{(1)} \bar{\mathbf{w}}_2 d\Gamma + \int_{\Gamma_3} \boldsymbol{\sigma}^{(f,2)}(\mathbf{w}^{(2)}) \cdot \mathbf{n}_s^{(2)} \bar{\mathbf{w}}_2 d\Gamma = 0. \tag{27}$$

Substituting of the Cauchy stress tensor Eq. (24) in Eqs. (26) and (27), we arrive at the weak form of the Stokes equation

$$\int_{\Omega_f^{(1)}} \rho_f^{(1)} \left[\frac{\partial^2 \mathbf{w}^{(1)}}{\partial t^2} \bar{\mathbf{w}}_1 + c_1^2 (\nabla \cdot \mathbf{w}^{(1)})(\nabla \cdot \bar{\mathbf{w}}_1) \right] d\Omega$$

$$+ 2\eta_1 \frac{\partial}{\partial t} \int_{\Omega_f^{(1)}} \left[\boldsymbol{\varepsilon}^{(f,1)}(\mathbf{w}^{(1)}) : \boldsymbol{\varepsilon}^{(f,1)}(\bar{\mathbf{w}}_1) - \frac{1}{3}(\nabla \cdot \mathbf{w}^{(1)})(\nabla \cdot \bar{\mathbf{w}}_1) \right] d\Omega$$

$$+ \int_{\Gamma_1} \boldsymbol{\sigma}^{(f,1)}(\mathbf{w}^{(1)}) \cdot \mathbf{n}_s^{(1)} \bar{\mathbf{w}}_1 d\Gamma = 0, \tag{28}$$

$$\int_{\Omega_f^{(2)}} \rho_f^{(2)} \left[\frac{\partial^2 \mathbf{w}^{(2)}}{\partial t^2} \bar{\mathbf{w}}_2 + c_2^2 (\nabla \cdot \mathbf{w}^{(2)})(\nabla \cdot \bar{\mathbf{w}}_2) \right] d\Omega$$

$$+ 2\eta_2 \frac{\partial}{\partial t} \int_{\Omega_f^{(2)}} \left[\boldsymbol{\varepsilon}^{(f,2)}(\mathbf{w}^{(2)}) : \boldsymbol{\varepsilon}^{(f,2)}(\bar{\mathbf{w}}_2) - \frac{1}{3}(\nabla \cdot \mathbf{w}^{(2)})(\nabla \cdot \bar{\mathbf{w}}_2) \right] d\Omega$$

$$+ \int_{\Gamma_2} \boldsymbol{\sigma}^{(f,2)}(\mathbf{w}^{(2)}) \cdot \mathbf{n}_s^{(1)} \bar{\mathbf{w}}_2 d\Gamma + \int_{\Gamma_3} \boldsymbol{\sigma}^{(f,2)}(\mathbf{w}^{(2)}) \cdot \mathbf{n}_s^{(2)} \bar{\mathbf{w}}_2 d\Gamma = 0. \tag{29}$$

2.4.2. *Solid domains*

In order to obtain a weak formulation for solid domains, firstly, Eq. (13) is multiplied by a test function $\bar{\mathbf{u}} = (\bar{\mathbf{u}}_1, \bar{\mathbf{u}}_2)$. Integrating by parts in $\Omega_s^{(i)}$ (i.e., using Green's formula for tensor fields) and taking into account the boundary conditions, we obtain

for inner solid (structure $\Omega_s^{(1)}$)

$$\int_{\Omega_s^{(1)}} \rho_s^{(1)} \frac{\partial^2 \mathbf{u}^{(1)}}{\partial t^2} \bar{\mathbf{u}}_1 d\Omega + \int_{\Omega_s^{(1)}} \boldsymbol{\sigma}^{(s,1)}(\mathbf{u}^{(1)}) : \boldsymbol{\varepsilon}^{(s,1)}(\bar{\mathbf{u}}_1) d\Omega$$

$$- \int_{\Gamma_1} \boldsymbol{\sigma}^{(f,1)}(\mathbf{w}^{(1)}) \cdot \mathbf{n}_s^{(1)} \bar{\mathbf{w}}_1 d\Gamma - \int_{\Gamma_2} \boldsymbol{\sigma}^{(f,2)}(\mathbf{w}^{(2)}) \cdot \mathbf{n}_s^{(1)} \bar{\mathbf{w}}_2 d\Gamma = 0 \qquad (30)$$

and for outer solid (vessel $\Omega_s^{(2)}$)

$$\int_{\Omega_s^{(2)}} \rho_s^{(2)} \frac{\partial^2 \mathbf{u}^{(2)}}{\partial t^2} \bar{\mathbf{u}}_2 d\Omega + \int_{\Omega_s^{(2)}} \boldsymbol{\sigma}^{(s,2)}(\mathbf{u}^{(2)}) : \boldsymbol{\varepsilon}^{(s,2)}(\bar{\mathbf{u}}_2) d\Omega$$

$$- \int_{\Gamma_3} \boldsymbol{\sigma}^{(f,2)}(\mathbf{w}^{(2)}) \cdot \mathbf{n}_s^{(2)} \bar{\mathbf{w}}_2 d\Gamma = 0. \qquad (31)$$

Applying the standard Galerkin discretization method, we have for a finite element

$$\mathbf{w}^{(1)} = \mathbf{H}_1^{(f)} \mathbf{W}_1, \quad \nabla \cdot \mathbf{w}^{(1)} = (\nabla \cdot \mathbf{H}_1^{(f)}) \mathbf{W}_1 = \mathbf{B}_1 \mathbf{W}_1,$$
$$\mathbf{w}^{(2)} = \mathbf{H}_2^{(f)} \mathbf{W}_2, \quad \nabla \cdot \mathbf{w}^{(2)} = (\nabla \cdot \mathbf{H}_2^{(f)}) \mathbf{W}_2 = \mathbf{B}_2 \mathbf{W}_2,$$
$$\mathbf{u}^{(1)} = \mathbf{H}_1^{(s)} \mathbf{U}_1, \quad \mathbf{u}^{(2)} = \mathbf{H}_2^{(s)} \mathbf{U}_2,$$

where $\mathbf{H}_1^{(f)}, \mathbf{H}_2^{(f)}, \mathbf{H}_1^{(s)}$ and $\mathbf{H}_2^{(s)}$ are the interpolation matrices, and $\mathbf{W}_1, \mathbf{W}_2, \mathbf{U}_1$ and $\mathbf{U}_2$ are the vectors of solution variables. By introducing $\boldsymbol{\mathcal{X}} = \{\mathbf{W}_1, \mathbf{W}_2, \mathbf{U}_1, \mathbf{U}_2\}^T$, discretization of the weak formulations (Eqs. (28)–(31)) induces a symmetrical system in $\mathbf{w}^{(1)}, \mathbf{w}^{(2)}, \mathbf{u}^{(1)}$ and $\mathbf{u}^{(2)}$ formulation as

$$(\boldsymbol{\mathcal{K}} + j\omega\boldsymbol{\mathcal{C}} - \omega^2 \boldsymbol{\mathcal{M}})\boldsymbol{\mathcal{X}} = \mathbf{0}, \qquad (32)$$

where $\boldsymbol{\mathcal{K}}, \boldsymbol{\mathcal{C}}$ and $\boldsymbol{\mathcal{M}}$ are the global stiffness, damping and mass matrices and

$$\boldsymbol{\mathcal{K}} = \begin{bmatrix} \mathbf{K}_1^{(f)} & \mathbf{O} & \mathbf{O} & \mathbf{O} \\ \mathbf{O} & \mathbf{K}_2^{(f)} & \mathbf{O} & \mathbf{O} \\ \mathbf{O} & \mathbf{O} & \mathbf{K}_1^{(s)} & \mathbf{O} \\ \mathbf{O} & \mathbf{O} & \mathbf{O} & \mathbf{K}_2^{(s)} \end{bmatrix}, \quad \boldsymbol{\mathcal{M}} = \begin{bmatrix} \mathbf{M}_1^{(f)} & \mathbf{O} & \mathbf{O} & \mathbf{O} \\ \mathbf{O} & \mathbf{M}_2^{(f)} & \mathbf{O} & \mathbf{O} \\ \mathbf{O} & \mathbf{O} & \mathbf{M}_1^{(s)} & \mathbf{O} \\ \mathbf{O} & \mathbf{O} & \mathbf{O} & \mathbf{M}_2^{(s)} \end{bmatrix}$$

$$\boldsymbol{\mathcal{C}} = \begin{bmatrix} \mathbf{C}_1^{(f)} - \mathbf{D}_1^{(f)} & \mathbf{O} & \mathbf{O} & \mathbf{O} \\ \mathbf{O} & \mathbf{C}_2^{(f)} - \mathbf{D}_2^{(f)} & \mathbf{O} & \mathbf{O} \\ \mathbf{O} & \mathbf{O} & \mathbf{O} & \mathbf{O} \\ \mathbf{O} & \mathbf{O} & \mathbf{O} & \mathbf{O} \end{bmatrix}$$

and the submatrices of Eq. (32) are defined by

$$\mathbf{K}_i^{(f)} = \int_{\Omega_f^{(i)}} \rho_f^{(i)} c_i^2 \mathbf{B}_i^T \mathbf{B}_i d\Omega,$$

$$\mathbf{U}_i^T \mathbf{K}_i^{(s)} \mathbf{U}_i = \int_{\Omega_s^{(i)}} \boldsymbol{\sigma}^{(s,i)}(\mathbf{u}^{(i)}) : \boldsymbol{\varepsilon}^{(s,i)}(\bar{\mathbf{u}}_i) d\Omega,$$

$$\mathbf{W}_i^T \mathbf{C}_i^{(f)} \mathbf{W}_i = \int_{\Omega_f^{(i)}} 2\eta_i \boldsymbol{\varepsilon}^{(f,i)}(\mathbf{w}^{(i)}) : \boldsymbol{\varepsilon}^{(f,i)}(\bar{\mathbf{w}}_i) d\Omega,$$

$$\mathbf{D}_i^{(f)} = \int_{\Omega_f^{(i)}} \frac{2\eta_i}{3} \mathbf{B}_i^T \mathbf{B}_i d\Omega,$$

$$\mathbf{M}_i^{(f)} = \int_{\Omega_i^{(f)}} \rho_f^{(i)} \mathbf{H}_i^{(f)T} \mathbf{H}_i^{(f)} d\Omega,$$

$$\mathbf{M}_i^{(s)} = \int_{\Omega_s^{(i)}} \rho_s^{(i)} \mathbf{H}_i^{(s)T} \mathbf{H}_i^{(s)} d\Omega.$$

2.4.3. *Finite element modeling*

In this section, the commercially available FEA package COMSOL Multiphysics[26] is used to solve the symmetrical Eq. (32). This modeling procedure requires two modules, one for simulating the elastic solids (structure and vessel) and the other for viscous fluids. Each module provides a wide range of equations, which is needed in specifying subdomains and boundaries. The theories and equations behind this model are based on the governing equations in Sec. 2. The solids and fluids are simulated using the Lagrange-Quadratic element and Lagrange-$P_2 P_1$ element, respectively. The solids and fluids elements at the interface shared the same node and have extremely fine meshing to capture the details during coupled vibrations.

The complete coupled system is simulated and presented in this section. Two modules (Fluid Flow and Structural Mechanics) are used in this simulation. For this purpose, some variables are set to make the connection between these two modules. At fluid–structure interface, kinematic and dynamic continuity has to be ensured. The complete coupled problem has to fulfill the condition that the location of the fluid–structure interface coincides for both fields. Thus, the fluid–structure interaction boundary condition concerning the fluid is of an inhomogeneous Dirichlet type (kinematic condition), and the fluid–structure boundary condition for the solids are given by an inhomogeneous Neumann condition (dynamic condition). For modeling of the coupled system, the eigenfrequency solver is selected to solve the model and give the first eleven eigenvalues. According to this solver, time for solving the model is 6.176 min and the number of degrees of freedom is 454919.

3. Results and Discussion

In this section, a numerical study is carried out to verify the validity of the theoretical method. We consider an elastic micro-structure filled with viscous fluid (inner fluid) enclosed within an elastic or rigid tube (vessel) shown in Fig. 1. The annulus between the tube is filled with viscous fluid (outer fluid). The geometry and material properties of the microstructures and the viscous fluid are presented in Table 1. In order to obtain the roots of the resulting frequency equation given in Eq. (21), the Mathematica software[27] is used. To validate the analytical results, the eigenvalues

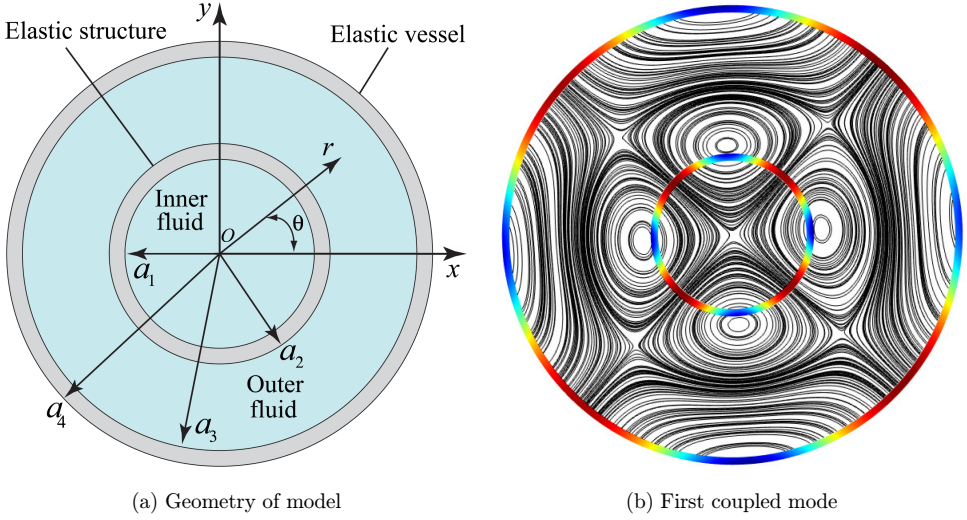(a) Geometry of model

(b) First coupled mode

Fig. 1. (a) Schematic describing the interaction of elastic micro-structures with a viscous fluids. (b) First coupled kinematic mode shape associated with the circumferential modal number $n = 2$.

and mode shapes are computed using Comsol Multiphysics Software. To simplify the presentation of results, natural frequencies are normalized and introduced as the nondimensional frequency, which is defined by $\omega a^2/\nu$. As it is known that the fluid-filled annular gap and elasticity of vessel affect the motion of the circular disk, an example is included to illustrate the effect of inner and outer fluids in conjunction with elasticity of tube. Table 2 shows the comparison of the first 11 frequencies by FEM and the theoretical calculation (Eq. (21)). The very good agreement is revealed between the results through the proposed method (Exact) and those of numerical

Table 1. Geometric and material properties.

Parameters of the system	Value
Inner fluid radius, $a_1 = a$	5 [μm]
Outer fluid radius, a_3	15 [μm]
Structure radius, a_2	5.5 [μm]
Elastic tube radius, a_4	15.5 [μm]
Inner fluid density, $\rho_0^{(1)}$	1000 [kg/m^3]
Outer fluid density, $\rho_0^{(2)}$	1000 [kg/m^3]
Inner fluid dynamic viscosity, η_1	0.01 [Pa·s]
Outer fluid dynamic viscosity, η_2	0.01 [Pa·s]
Structure material density, $\rho_s^{(1)}$	1200 [kg/m^3]
Tube material density, $\rho_s^{(2)}$	1200 [kg/m^3]
Structure material Young's modulus, E_1	$2 \cdot 10^6$ [Pa]
Tube material Young's modulus, E_2	$6 \cdot 10^7$ [Pa]
Structure material Poisson's ratio, ν_1	0.4
Tube material Poisson's ratio, ν_2	0.4

Table 2. Nondimensional natural frequencies $\frac{\omega a^2}{\nu}$ with a fluid filled rigid vessel.

	In vacuum			Outer fluid only			Outer and inner fluid	
n	Exact	FEM	n	Exact	FEM	n	Exact	FEM
2	1.557	1.557	2	0.060	0.060	2	0.040	0.040
3	4.367	4.367	3	0.456	0.456	3	0.238	0.238
4	8.275	8.275	4	1.338	1.338	4	0.621	0.621
5	13.188	13.188	0	1.774	1.774	5	1.227	1.227
6	19.015	19.015	5	2.764	2.764	0	1.627	1.627
0	21.240	21.240	1	4.655	4.655	6	2.087	2.087
7	25.668	25.668	6	4.824	4.824	7	3.221	3.221
1	29.961	29.961	7	7.612	7.612	1	3.862	3.862
8	33.057	33.057	8	11.206	11.206	8	4.639	4.639
9	41.096	41.096	9	15.661	15.661	9	6.342	6.342
10	49.705	49.705	10	20.999	20.999	10	8.322	8.322

solution (FEM) and the mode shapes are not in order with the parameter n. Table 2 shows also that the fundamental frequency is always with the $n = 2$. In the following, we study the nondimensional frequency curves of $n = 2$ with the changing of the other models parameters.

3.1. *Effects of inner fluid, outer fluid gap and elastic vessel*

In the analysis, two cases are inspected. First case is when only the outer annular fluid is considered, and the second case is when the elastic micro-disc is coupled with outer annular fluid and inner fluid. The nondimensional frequency $\omega a^2/\nu$ is plotted versus circumferential mode number n in Fig. 2. For smaller values of circumferential mode number, the difference of the nondimensional frequencies between the two cases is relatively small. Nevertheless, when circumferential mode number increases, this difference increases also. In other words, the inner fluid relatively affects the nondimensional frequencies for higher circumferential modes, and the outer annular
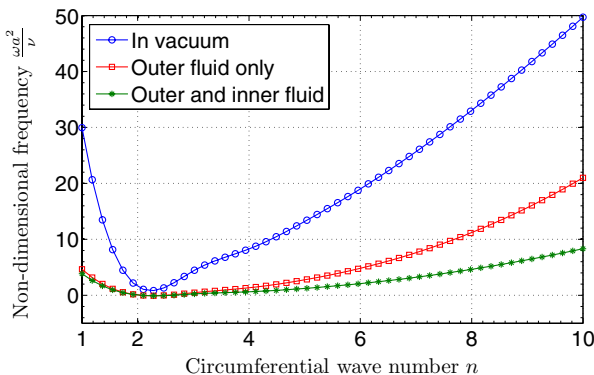

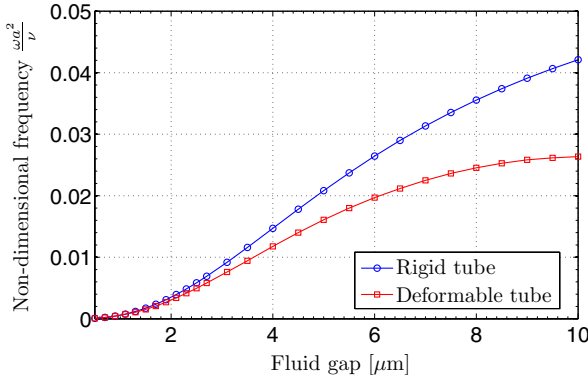Fig. 2. Nondimensional frequency curves $\omega a^2/\nu$ versus n.

Fig. 3. Variation of nondimensional frequency of first mode ($n = 2$) versus fluid gap for the two models (rigid and deformable tube (vessel)).

fluid affects those of lower circumferential modes. Furthermore, it is expected that the difference between the nondimensional frequency of the two cases may be accelerated when we reduce the outer fluid gap. This effect of the outer fluid gap is shown in Fig. 3 for the two models. This figure shows that the nondimensional frequencies increase with the outer fluid gap. In other words, a narrow gap tends to reduce the nondimensional frequencies. When the fluid gap $a_3 - a_2$ is less than about 2, the natural frequencies are not affected by the stiffness of the tube. This behavior is also found for second coupled mode ($n = 3$). However, the stiffness of the tube is very significant when the fluid gap $a_3 - a_2$ is greater than 4. A swirling of fluid along the structure edge will make change in fluid velocity and it will decrease the natural frequencies due to an increase of the added mass.

The effect of elastic tube (vessel) on the natural frequencies is shown in Fig. 4 for the two cases. The main effect of the constraint imposed on an elastic fluid-filled tube by an elastic micro-structure filled with compressible fluid is to reduce the natural frequencies. This behavior is also found for second coupled mode ($n = 3$). The main
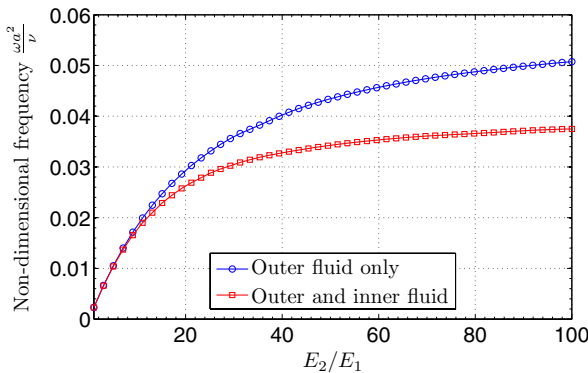

Fig. 4. Variation of nondimensional frequency of first mode ($n = 2$) versus Young's modulus ratio.

reason is the increase of the effective radial inertia due to the normal stresses in the fluid in the annulus, necessary to maintain the constant volume in the system. For the lower elasticity ratio E_2/E_1, the difference of the nondimensional natural frequencies is relatively small between the two cases. However, the difference increases with increasing elasticity ratio and converges to the asymptotic value found in the case of the rigid tube (Table 2).

3.2. *Modes shapes*

In order to verify the validity of coupled formulation for fluid–structure analysis implemented in the Comsol Multiphysics software, it is checked in Figs. 5–7 that the

(a) First mode $n = 2$ (b) First mode $n = 3$
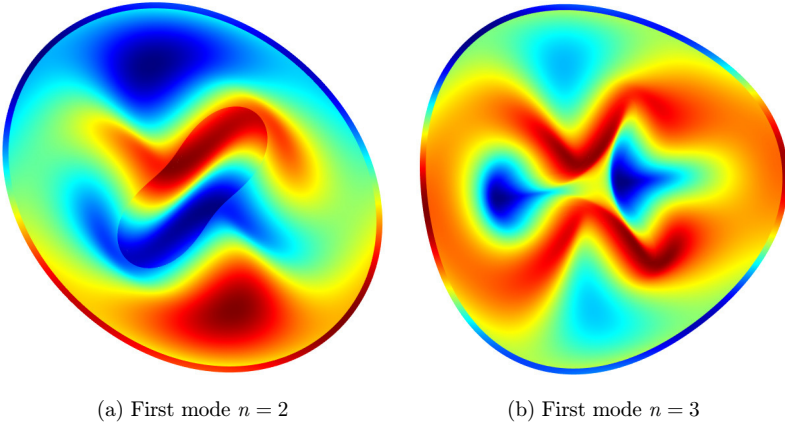
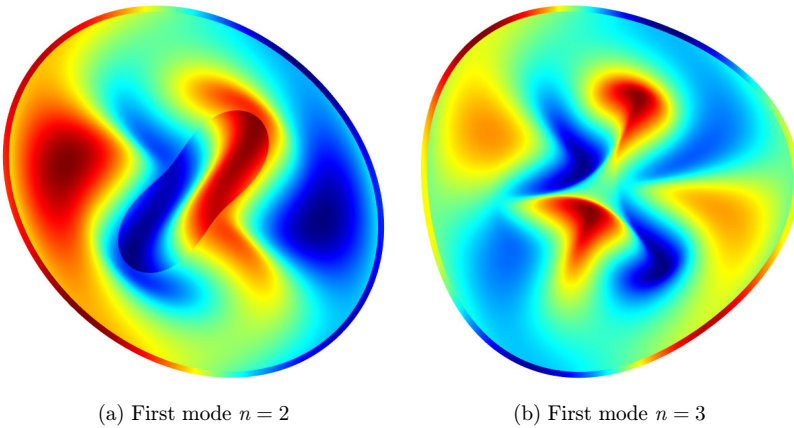Fig. 5. Continuity of the two first x-component of velocity field associated with the circumferential modal number.

(a) First mode $n = 2$ (b) First mode $n = 3$

Fig. 6. Continuity of the two first y-component of velocity field associated with the circumferential modal number.

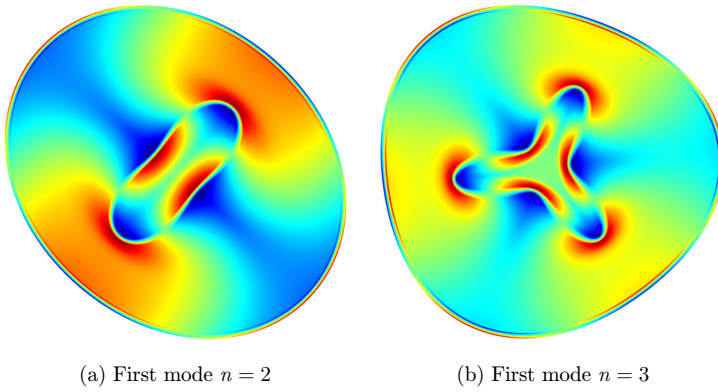(a) First mode $n = 2$ (b) First mode $n = 3$

Fig. 7. Continuity of the normal stress associated with the circumferential modal number.

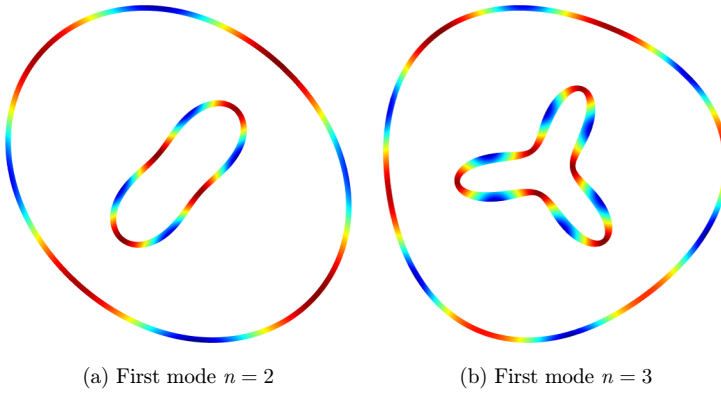(a) First mode $n = 2$ (b) First mode $n = 3$

Fig. 8. Two first structure $(i = 1)$ and vessel $(i = 2)$ deformed kinematic mode shapes for the deformable vessel model associated with the circumferential modal number.
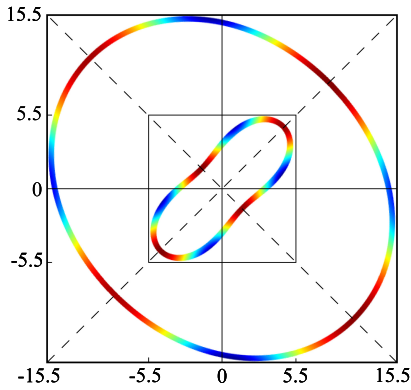

Fig. 9. First mode shapes for the circumferential wavenumber $n = 2$, 9 0 ° out of phase.

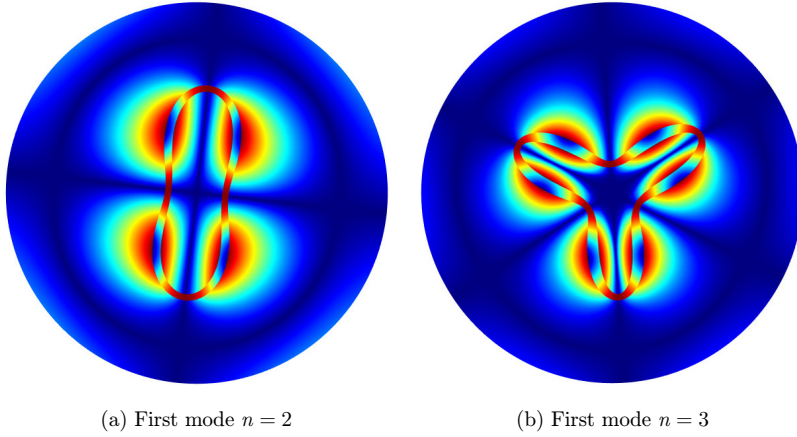(a) First mode $n = 2$ (b) First mode $n = 3$

Fig. 10.   Two first coupled deformed kinematic mode shapes for the rigid vessel model associated with the circumferential modal number. The color for fluid domain corresponds to the vorticity magnitude and the color for solid domain corresponds to the velocity magnitude.

velocity, displacement and stress are accurately calculated : the fluid velocity and solid velocity are identical, normal fluid stress and normal structure stress are identical, in accordance with the boundary conditions Eqs. (18) and (19). In addition, the first and second serial modes of the circumferential mode number $n = 2$ and $n = 3$ are typical apparent $90°$ out of phase modes, as shown in Figs. 8 and 9. Furthermore, Figs. 10 and 11 show the link between the vorticity and the mode shape. Indeed, the deformed wall is due to the pressure and vorticity fields. It should also be noted that for the structure, the kinematic deformations are homothetic to the spatial deformations because $\partial u / \partial t = j\omega u$. Furthermore, Fig. 12 shows the presence of Stokes eddies in the case of a rigid vessel. These Stokes eddies cross the
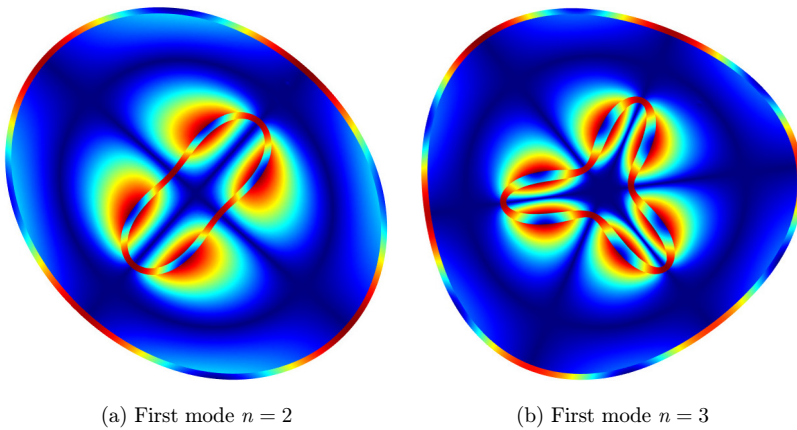

(a) First mode $n = 2$ (b) First mode $n = 3$

Fig. 11.   Two first coupled deformed kinematic mode shapes for the deformable vessel model associated with the circumferential modal number.
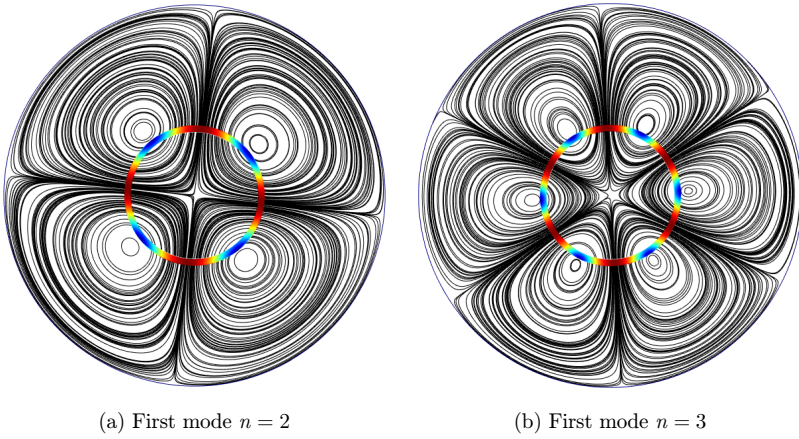
(a) First mode $n = 2$ (b) First mode $n = 3$

Fig. 12.   Streamlines of the first two eigenmodes for the rigid vessel model associated with the circumferential modal number.

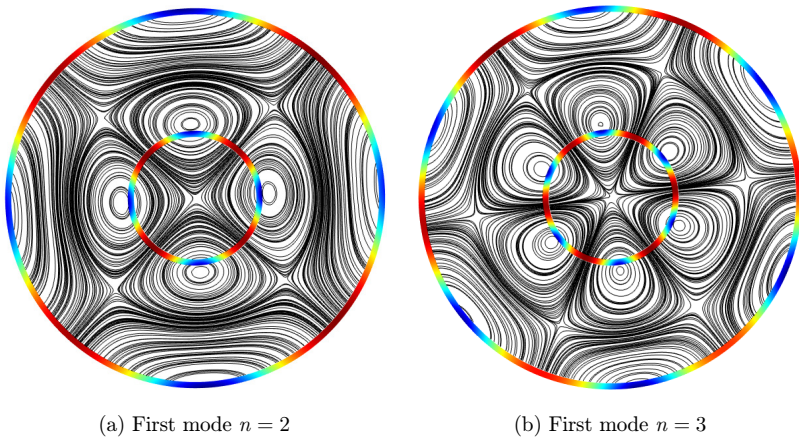(a) First mode $n = 2$ (b) First mode $n = 3$

Fig. 13.   Streamlines of the first two eigenmodes for the deformable vessel model associated with the circumferential modal number.

microstructure due to the no slip wall condition and to the mass conservation across the fluids-microstructure interface. However, when the vessel wall was assumed to be elastic, the Stokes eddies will migrate to the inside of the domain, as shown in Fig. 13. Indeed, the vessel wall is no longer a streamline, but a flow source, where the velocities of the fluid particles are no longer equal to zero.

4. Conclusion

The characteristics of vibration analysis of two micro-circular disks subjected to compressible fluid, based on the linear two-dimensional elasticity theory are

investigated. The Helmholtz decomposition theorem is employed to formulate the solution for free in-plane vibrations of the micro-circular disks. The coupled natural frequencies of vibration of the microdisks-fluids system were studied theoretically and numerically. A numerical model (FEM) was developed using the Comsol Multiphysics software. The very good agreement is revealed between the results through the proposed method and those of numerical solution. The effects of outer and inner fluids on the natural frequency is investigated in order to evaluate the modal behavior of the microdisks-fluids system. It is found that the inner fluid tends to reduce the nondimensional frequencies for higher circumferential modes, and the outer fluid tends to reduce those of lower circumferential modes. Furthermore, the results obtained in this paper can serve as benchmark solutions and as a reference to assess the accuracy of approximate methods. Additionally, the studying of the viscoelastic effects should be explored in future work.

Appendix A

Expressions for the sub-matrices $\mathbf{M}_q^{(i)}(r)$:

To make it clear and simple, the components of velocity, displacement and stress tensor are presented in the following form:

$$
\text{for fluid domain}: \begin{Bmatrix} v_r^{(i)}(r) \\ v_\theta^{(i)}(r) \\ \sigma_{rr}^{(f,i)}(r) \\ \sigma_{r\theta}^{(f,i)}(r) \end{Bmatrix} = \begin{bmatrix} v_1^{(i)}(r) & v_2^{(i)}(r) & -v_3^{(i)}(r) & -v_4^{(i)}(r) \\ v_5^{(i)}(r) & v_6^{(i)}(r) & -v_7^{(i)}(r) & -v_8^{(i)}(r) \\ F_1^{(i)}(r) & F_2^{(i)}(r) & -F_3^{(i)}(r) & -F_4^{(i)}(r) \\ F_5^{(i)}(r) & F_6^{(i)}(r) & -F_7^{(i)}(r) & -F_8^{(i)}(r) \end{bmatrix} \begin{Bmatrix} A_f^{(i)} \\ B_f^{(i)} \\ C_f^{(i)} \\ D_f^{(i)} \end{Bmatrix}
$$

$$
\text{for solid domain}: \begin{Bmatrix} u_r^{(i)}(r) \\ u_\theta^{(i)}(r) \\ \sigma_{rr}^{(s,i)}(r) \\ \sigma_{r\theta}^{(s,i)}(r) \end{Bmatrix} = \begin{bmatrix} u_1^{(i)}(r) & u_2^{(i)}(r) & -u_3^{(i)}(r) & -u_4^{(i)}(r) \\ u_5^{(i)}(r) & u_6^{(i)}(r) & -u_7^{(i)}(r) & -u_8^{(i)}(r) \\ S_1^{(i)}(r) & S_2^{(i)}(r) & -S_3^{(i)}(r) & -S_4^{(i)}(r) \\ S_5^{(i)}(r) & S_6^{(i)}(r) & -S_7^{(i)}(r) & -S_8^{(i)}(r) \end{bmatrix} \begin{Bmatrix} A_s^{(i)} \\ B_s^{(i)} \\ C_s^{(i)} \\ D_s^{(i)} \end{Bmatrix}
$$

The detailed expressions of the sub-matrices $\mathbf{M}_q^{(i)}(r)$ in Eq. (22) are defined as follow:

$$
\mathbf{M}_f^{(1)}(a_1) = \begin{bmatrix} v_1^{(1)}(a_1) & -v_3^{(1)}(a_1) \\ v_5^{(1)}(a_1) & -v_7^{(1)}(a_1) \\ F_1^{(1)}(a_1) & -F_3^{(1)}(a_1) \\ F_5^{(1)}(a_1) & -F_7^{(1)}(a_1) \end{bmatrix},
$$

$$\mathbf{M}_f^{(i)}(r) = \begin{bmatrix} v_1^{(i)}(r) & v_2^{(i)}(r) & -v_3^{(i)}(r) & -v_4^{(i)}(r) \\ v_5^{(i)}(r) & v_6^{(i)}(r) & -v_7^{(i)}(r) & -v_8^{(i)}(r) \\ F_1^{(i)}(r) & F_2^{(i)}(r) & -F_3^{(i)}(r) & -F_4^{(i)}(r) \\ F_5^{(i)}(r) & F_6^{(i)}(r) & -F_7^{(i)}(r) & -F_8^{(i)}(r) \end{bmatrix} \quad \text{for } r = a_2, a_3,$$

$$\mathbf{M}_s^{(i)}(r) = \begin{bmatrix} \alpha^2 u_1^{(i)}(r) & \alpha^2 u_2^{(i)}(r) & \alpha^2 u_3^{(i)}(r) & \alpha^2 u_4^{(i)}(r) \\ \alpha^2 u_5^{(i)}(r) & \alpha^2 u_6^{(i)}(r) & \alpha^2 u_7^{(i)}(r) & \alpha^2 u_8^{(i)}(r) \\ -S_1^{(i)}(r) & -S_2^{(i)}(r) & S_3^{(i)}(r) & S_4^{(i)}(r) \\ -S_5^{(i)}(r) & -S_6^{(i)}(r) & S_7^{(i)}(r) & S_8^{(i)}(r) \end{bmatrix} \quad \text{for } r = a_1, a_2, a_3,$$

$$\mathbf{M}_s^{(2)}(a_4) = \begin{bmatrix} S_1^{(2)}(a_4) & S_2^{(2)}(a_4) & -S_3^{(2)}(a_4) & -S_4^{(2)}(a_4) \\ S_5^{(2)}(a_4) & S_6^{(2)}(a_4) & -S_7^{(2)}(a_4) & -S_8^{(2)}(a_4) \end{bmatrix}.$$

The elements in the sub-matrices $\mathbf{M}_q^{(i)}(r)$ are calculated according to the following formulations:

$$(v_1^{(i)}, v_2^{(i)})(r) = (J_n', Y_n')(\beta_i r),$$

$$(v_3^{(i)}, v_4^{(i)})(r) = \frac{n}{r}(J_n, Y_n)\left(\frac{\alpha r}{\sqrt{\nu_i}}\right),$$

$$(v_5^{(i)}, v_6^{(i)})(r) = \frac{n}{r}(J_n, Y_n)(\beta_i r),$$

$$(v_7^{(i)}, v_8^{(i)})(r) = (J_n', Y_n')\left(\frac{\alpha r}{\sqrt{\nu_i}}\right),$$

$$(F_1^{(i)}, F_2^{(i)})(r) = 2\eta_i\left[(J_n'', Y_n'') + \left(\beta_i^2 - \frac{\alpha^2}{2\nu_i}\right)(J_n, Y_n)\right](\beta_i r),$$

$$(F_3^{(i)}, F_4^{(i)})(r) = 2\eta_i\frac{n}{r^2}[r(J_n', Y_n') - (J_n, Y_n)]\left(\frac{\alpha r}{\sqrt{\nu_i}}\right),$$

$$(F_5^{(i)}, F_6^{(i)})(r) = \eta_i\frac{2n}{r^2}t[r(J_n', Y_n') - (J_n, Y_n)](\beta_i r),$$

$$(F_7^{(i)}, F_8^{(i)})(r) = \eta_i\left[2(J_n'', Y_n'') + \frac{\alpha^2}{\nu_i}(J_n, Y_n)\right]\left(\frac{\alpha r}{\sqrt{\nu_i}}\right),$$

$$(u_1^{(i)}, u_2^{(i)})(r) = (I_n', K_n')(k_L^{(i)} r),$$

$$(u_3^{(i)}, u_4^{(i)})(r) = \frac{n}{r}(I_n, K_n)(k_T^{(i)} r),$$

$$(u_5^{(i)}, u_6^{(i)})(r) = \frac{n}{r}(I_n, K_n)(k_L^{(i)} r),$$

$$(u_7^{(i)}, u_8^{(i)})(r) = (I_n', K_n')(k_T^{(i)} r),$$

$$(S_1^{(i)}, S_2^{(i)})(r) = [2\mu_i(I_n'', K_n'') + \lambda_i k_L^{(i)2}(I_n, K_n)](k_L^{(i)}r),$$

$$(S_3^{(i)}, S_4^{(i)})(r) = \mu_i \frac{2n}{r^2}[r(I_n', K_n')(k_T^{(i)}r) - (I_n, K_n)(k_T^{(i)}r)],$$

$$(S_5^{(i)}, S_6^{(i)})(r) = \mu_i \frac{2n}{r^2}[r(I_n', K_n')(k_L^{(i)}r) - (I_n, K_n)(k_L^{(i)}r)],$$

$$(S_7^{(i)}, S_8^{(i)})(r) = \mu_i[2(I_n'', K_n'')(k_T^{(i)}r) - k_T^{(i)2}(I_n, K_n)(k_T^{(i)}r)],$$

where primes denote differentiation with respect to the position variable r.

References

1. M. P. Paidoussis and G. X. Li, Pipes conveying fluid: A model dynamical problem, *J. Fluids Struct.* **7** (1993) 137–204.
2. M. P. Paidoussis, *Fluid-Structure Interactions: Slender Structures and Axial Flow*, Vol. 1 (London Academic Press, 1998).
3. J. Pihl, M. Karlsson and D. T. Chiu, Microfluidic technologies in drug discovery, *Drug Discov. Today* **10** (2005) 1377–1383.
4. D. R. Reyes, D. Lossifidis, P. A. Auroux and A. Manz, Micro total analysis systems. 1. introduction, theory, and technology, *Anal. Chem.* **74** (2002) 2623–2636.
5. P. A. Auroux, D. Lossifidis, D. R. Reyes and A. Manz, Micro total analysis systems. 2. Analytical standard operations and applications, *Anal. Chem.* **74** (2002) 2637–2652.
6. M. Najmzadeh, S. Haasl and P. Enoksson, A silicon straight tube fluid density sensor, *J. Micromech. Microeng.* **17** (2007) 1657–1663.
7. A. A. Bhirde, V. Patel, J. Gavard, G. Zhang, A. A. Sousa, A. Masedunskas, R. D. Leapman, R. Weigert, J. Silvio Gutkind and J. F. Rusling, Targeted killing of cancer cells *in vivo* and *in vitro* with EGF-directed carbon nanotube-based drug delivery, *ACS Nano* **3** (2009) 307–316.
8. A. D. Van Der Meer, A. A. Poot, M. H. G. Duits, J. Feijen and I. Vermes, Microfluidic technology in vascular research, *J. Biomed. Biotechnol.* **2009** (2009) Article ID 823148, 10 pages.
9. D. Abreu, M. Levant, V. Steinberg and U. Seifert, Fluid vesicles in flow, *Adv. Colloid Interface Sci.* **208** (2014) 129–141.
10. U. Seifert, Configurations of fluid membranes and vesicles, *Advances in Physics* **46** (1997) 13–137.
11. D. Barthès-Biesel, Modeling the motion of capsules in flow, *Curr. Opin. Coll. Interf. Sci.* **16** (2011) 3–12.
12. P. M. Vlahovska, T. Podgorski and C. Misbah, Vesicles and red blood cells: From individual dynamics to rheology, *Comptes Rendus Physique* **10** (2009) 775–789.
13. X. Li, P. M. Vlahovskab and G. E. Karniadakis, Continuum- and particle-based modeling of shapes and dynamics of red blood cells in health and disease, *Soft Matter* **9** (2013) 28–37.
14. J. B. Freund, Numerical simulation of flowing blood cells, *Annu. Rev. Fluid Mech.* **46** (2014) 67–95.
15. L. D. Landau and E. M. Lifshitz, *Fluid Mechanics* (Pergamon Press, 1959).
16. M. Morse and H. R. Feshbach, *Methods of Theoretical Physics* (McGraw-Hill, New York, 1946).
17. I. Mnassri and A. El Baroudi, Vibrational frequency analysis of finite elastic tube filled with compressible viscous fluid, *Acta Mech. Solida Sin.* **30** (2017) 435–444.

18. J. D. Achenbach, *Wave Propagation in Elastic Solids* (North-Holland, The Netherlands, 1975).
19. A. A. Parthasarathi, K. Grosh and A. L. Nuttall, Three-dimensional numerical modeling for global cochlear dynamics, *J. Acoust. Soc. Am.* **107** (2000) 474–485.
20. H. J. P. Morand and R. Ohayon, Substructure variational analysis of the vibrations of coupled fluid-structure systems: Finite element results, *Int. J. Numer. Methods Eng.* **14** (1979) 741–755.
21. M. A. Hamdi, Y. Ousset and G. Verchery, A displacement method for analysis of vibrations of coupled fluid-structure systems, *Int. J. Numer. Methods Eng.* **13** (1978) 139–150.
22. K. J. Bathe, *Finite Element Procedures* (Prentice Hall, NY, 1996).
23. M. Mellado and R. Rodriguez, Efficient solution of fluid-structure vibration problems, *Appl. Numer. Math.* **36** (2001) 389–400.
24. O. C. Zienkiewich and R. L. Taylor, *The Finite Element Method*, Vol. 2 (McGraw-Hill, 1989).
25. H. J. P. Morand and R. Ohayon, *Fluid Structure Interaction* (John Wiley & Sons, NY, 1995).
26. Comsol Multiphysics User's Guide, Version 3.5a (Stockholm, Sweden, 2008).
27. Wolfram Research Mathematica, User's Manual Version 10.1, Champaign, Illinois (2015).